Evaluation of equivalent friction damping ratios at bearings of welded large-scale single-layer lattice domes subjected to earthquake ground motions

Huidong Zhang[*1,2], Xinqun Zhu[3] and Shu Yao[1,2]

[1]*Tianjin Key Laboratory of Civil Buildings Protection and Reinforcement, Tianjin 300384, PR China*
[2]*School of Civil Engineering, Tianjin Chengjian University, Tianjin 300384, PR China*
[3]*School of Civil and Environmental Engineering, University of Technology Sydney, NSW 2007, Australia*

(Received keep as blank , Revised keep as blank , Accepted keep as blank)

Abstract. The major sources of damping in steel structures are within the joints and the structural material. For welded large-scale single-layer lattice domes subjected to earthquake ground motions, the stick-slip phenomenon at the bearings is an important source of the energy dissipation. However, it has not been extensively investigated. In this study, the equivalent friction damping ratio (EFDR) at the bearings of a welded large-scale single-layer lattice dome subjected to earthquake ground motions is quantified using an approximate method based on the energy balance concept. The complex friction behavior and energy dissipation between contact surfaces are investigated by employing an equivalent modeling method. The proposed method uses the stick-slip-hook components with a pair of circular isotropic friction surfaces having a variable friction coefficient to model the energy loss at the bearings, and the effect of the normal force on the friction force is also considered. The results show that the EFDR is amplitude-dependent and is related to the intensity of the ground motions; it exhibits complex characteristics that cannot be described by the conventional models for damping ratios. A parametric analysis is performed to investigate in detail the effects of important factors on the EFDR. Finally, the friction damping mechanism at bearings is discussed. This study enables researchers and engineers to have a better understanding of the essential characteristics of friction damping under earthquake ground motions.

Keywords: equivalent damping ratio; friction; large-scale single-layer lattice dome; bearing; variable friction coefficient.

1. Introduction

Damping appears in several forms in steel structures and may be broadly categorized as external and internal (Beards 1996). External damping occurs in active control systems, such as damping devices used to reduce the vibration of a structure, and boundary effects, such as the loss of energy at the bearings through either friction or transmission into the supporting structure (Zhang *et al.* 2016). Internal damping includes the internal friction of materials and the friction at the joints (Sheen 1984). From the perspective of material damping, some scholars have conducted extensive research (Gounaris and Anifantis 1999, Goodman 2002, Lazan 1968, Gounaris and Antonakakis *et al*. 2007, Zhang and Wang *et al*. 2015).

The connection measures between components in steel structures mainly include the welded connection, bolted connection, and mixed connections. For the latter two connections, most of the internal damping in the structure originates from the bolted parts. It is reported that the damping at the bolted connections accounts for 80–90% of the total structural damping, which is due to the small slip of the contact interfaces at the bolted connections (Beards 1996). In bolted structures, the stick-slip phenomena at connections are the most important source of damping (Zhang *et al.* 2019). However, for welded steel structures, the slip damping at the connections of the structure is almost nonexistent. Therefore, the damping ratio of bolted structures is much larger than that of welded steel structures. Clarence (2005) reported that the American Society of Mechanical Engineers (ASME) proposes that the damping ratio of welded steel structures subjected to earthquake ground motions is 2–4%, while that of bolted structures is 4–7%. The quantification of damping in structures has always been an important and challenging issue (Kareem and Gurley 1996). It should be noted that the assessment of damping can only be approximate, and it is difficult to obtain accurate and reliable test data, particularly in the region of resonance, because the analysis for damping will depend upon whether viscous or hysteretic damping is assumed, and some non-linearity may occur in real systems.

There are two important approaches to describing damping from a mathematical perspective. The most commonly used damping quantification method is the amplitude decay method based on free vibrations (Feeny and Liang 1996), wherein the rate of decay depends on the degree of damping. The damping ratios obtained in this way are the viscous mode damping ratios of structures with small amplitudes. Another damping description is defined by an equivalent damping ratio (EDR), which is based on the ratio of the nonlinear dissipated energy and the elastic stored energy, and which was originally proposed by Lydik Jacobsen (Jacobsen 1930). This method can quantify the

damping of structures with larger amplitudes. It should be noted the Jacobsen's EDR depends on the displacement amplitude, whereas viscous damping is proportional to the velocity. Although the concept of the modal damping ratio, which is a percentage of the critical damping, is strictly applicable only for linear structural behavior, it is possible to calculate an approximate EDR for nonlinear behavior (Feeny and Liang 1996). However, the modal damping ratios obtained by the low-amplitude forced vibration tests are not representative of the larger damping expected at higher amplitudes of structural motions. In dynamic analysis, the data that are most useful but difficult to obtain are from structures that are shaken strongly without being deformed into the inelastic range (Chopra 2011). At present, the procedure that is most commonly used to estimate the EDR of a structure subjected to earthquake ground motions is Jacobsen's approach. Based on the viscous damping assumptions and Jacobsen's equivalent damping quantification method, many researchers (Kwan and Billington 2003, Liu *et al.* 2015, Papagiannopoulos 2018, Dwairi and Kowalsky 2007, Papagiannopoulos and Beskos 2010, Jennings 1968) have evaluated the EDRs of structures and investigated the displacement-prediction capacity of equivalent linear structures in a direct displacement-based seismic design (DDBSD) framework. From a practical perspective, the EDR represents the overall damping behavior of a structural system subjected to dynamic loads, and is often used in structural dynamic analyses (Tamura 2012).

When a structure connected to a foundation is subjected to dynamic loads, there are inevitably some dry friction phenomena in the connection area (or at the bearings), which include the slip friction from the steel–steel contact surfaces and the contact between the bearings and the foundation (or supports), the dry friction caused by the contact between the foundation and the surrounding soil (or concrete) media, and special bearings that rely on friction mechanisms to dissipate energy. Based on the above discussion, two main sources of damping occur in welded large-scale single-layer lattice domes without shock-absorption and isolation devices (the radiation damping at supports is not considered in this study): (i) internal damping: the damping of the steel material itself; (ii) external damping: the small slip damping at surfaces making contact at bearings. It is found that the structural damping ratio contributed by the material itself is very small in welded large-scale single-layer lattice domes subjected to earthquake ground motions (Zhang, Wang, and Han 2015), while the damping ratio contributed by the friction behavior at bearings of the structure may be larger; therefore, the friction at bearings is an important damping source for welded large-scale single-layer domes. However, this external friction damping source has not been extensively studied and quantified for structures subjected to earthquake ground motions.

A previous study indicates that the friction mechanism consists of frictional stick and slip between the interfaces, and the energy loss per cycle due to friction is independent of the excitation frequency (Zhang *et al.* 2019). Unlike the viscous damping, it is difficult to quantify the friction damping ratio because of its amplitude-dependent characteristic. In spite of the extensive research on damping models, the use of the viscous damping model in friction damping continues to be debated because it is not strictly related to the physics behind the friction damping mechanism (Petrini *et al.* 2008). For a dynamic analysis related to friction behaviors, the friction phenomena should theoretically be directly modeled by the nonlinear force-deformation relationships.

In this study, the energy dissipation due to friction at each bearing of a welded large-scale single-layer lattice dome is first explicitly modeled using an equivalent stick-slip-hook component (Zhang and Zhu 2019) with a circular isotropic friction surface that can slide horizontally; this component is used to consider the overall friction damping behavior at each bearing. Secondly, an energy analysis for the welded large-scale single-layer lattice dome with friction components subjected to earthquake ground motions is performed based on the energy balance concept. Then, the EDRs resulting from the friction at the bearings are evaluated based on a further-developed Jacobsen's approach, and a parametric study is performed by considering the effects of different factors on the EDR. Finally, the friction damping mechanism at the bearings is discussed.

2. Methods

2.1 Dynamics equation

For a nonlinear structure with multiple-degrees of freedom, the dynamic equation can be described as

$$[M]\{\ddot{x}\} + \{F_d\} + [K]\{x\} + \{F_f\} = \{p(t)\} \quad (1)$$

where $[M]$ and $[K]$ are the mass and stiffness matrices, respectively; $\{\ddot{x}\}$, $\{F_d\}$, $\{x\}$, and $\{F_f\}$ are the nodal acceleration, viscous damping force, displacement, and friction force vectors, respectively; and $\{p(t)\}$ is the external force vector of the structure. The energy-based balance formulation for the above structure can be found in (Zhang and Wang (2012a). Its form is as follows:

$$E_K(t) + E_D(t) + E_F(t) + E_S(t) + E_H(t) = E_I(t) \quad (2)$$

where $E_I(t)$ is the input energy applied to the structure; $E_K(t)$ and $E_S(t)$ are the kinetic and recoverable strain energy values of the structure, respectively; and $E_D(t)$, $E_F(t)$, and $E_H(t)$ are the energy dissipation due to viscous damping, energy dissipation due to friction, and hysteretic energy dissipation, respectively. Among them, the hysteretic energy dissipation due to yielding can be directly accounted for separately using nonlinear force–deformation (or stress–strain) relationships. Finally, the total input energy is completely dissipated by the viscous damping, friction, and hysteresis during an earthquake. Eq. (2) can be rewritten as

$$E_D + E_F + E_H = E_I \quad (3)$$

where E_D, E_F, E_H, and E_I represent the total viscous damping energy dissipation, total friction energy dissipation,

Table 1 Properties of the ESMS

Mass	m=10 kg	Stick stiffness	k_1=50000 N/m
Spring stiffness	k_0= 2000 N/m	Hook stiffness	k_2=80000 N/m
Normal force	P= 200 N	Stick distance	$x_1=\mu P/k_1$=2e-3 m
Friction coefficient	μ=0.5	Stick-slip distance	x_2=0.01 m
Modal damping ratio	ξ_0=5%	Mode period	T=0.4531 s

total hysteresis energy, and total input energy, respectively. The structural EDR ξ obtained using the energy-based damping definition can be written as (Jacobsen 1930)

$$\xi = \frac{1}{4\pi}\sum_{i=1}^{n} E_{d,i}/E_{s,max}. \quad (4)$$

where $E_{d,i}$ is the energy dissipation of the ith damping source in one cycle; n is the total number of damping sources; and $E_{s,max}$ is the maximum strain energy of the structure in a complete cycle. At this point, it is clear that the EDR of a system depends not only on the dissipated energy, but also on the maximum strain energy.

2.2 Approximate overall quantification method for damping ratio

For a structure subjected to an earthquake ground motion, the strain energy of the structure varies with time during the earthquake. Each strain energy peak approximately corresponds to a half cycle, as shown in Fig. 1. If we assume that the mean of the strain energy peaks is 2 times the mean strain energy, an approximate estimation for the EDR can be calculated as (Computers and Structures 1995)

$$\xi = \frac{1}{4\pi N}\sum_{i=1}^{n} E_{d,i}\Big/\bar{E}_s \quad (5)$$

where $\bar{E}_s$ is the mean strain energy during an earthquake, and N is the total number of half cycles (strain energy peaks).

This method was proposed in the literature (Computers and Structures 1995) and has been used to evaluate the equivalent viscous damping ratios for the hysteretic energy of elastoplastic structures subjected to earthquake ground motions (Zhang and Wang 2012a, b).

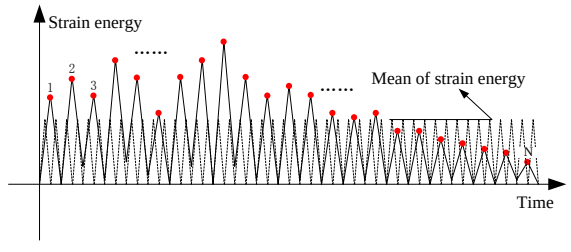

Fig. 1 Equivalent estimation method for damping ratio

3. Verification

The feasibility of the above approximate quantification method for the friction damping was verified using an elastic spring–mass system (ESMS), as shown in Fig. 2. Case 1 represents the system with friction damping at the support, where the friction damping is modeled using a stick-slip-hook component. The system has a modal damping ratio of 5%, and the seismic energy acting on the system is dissipated by both modal damping and friction. Case 2 that has an additional damping is the equivalent for Case 1. In Case 2, the support is fixed, and the seismic energy is dissipated by equivalent damping that includes both the modal and friction damping in Case 1. The properties of the ESMS are listed in Table 1. The normal force P is constant. The stiffness of the system k is equal to $k_0k_1/(k_0+k_1)$, which is 1923 N/m. The nonlinear system is excited using three earthquake ground motions listed in Table 2, respectively.

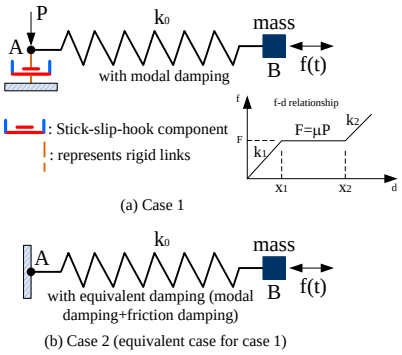

Fig. 2 Two cases of ESMS

Table 2 Three earthquake ground motions

Ground motions	PGA	Scale factor	Duration /s
El-Centro 1940 (E-W)	0.8592g	1	25
Northridge (14145 Mulholland, E-W)	0.5165g	1	25
Loma Prieta (Gilroy station 1, E-W)	0.9462g	1	10

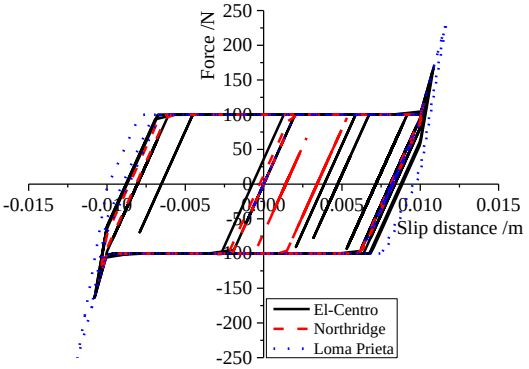

Fig. 3 Hysteresis curves of the stick-slip-hook component

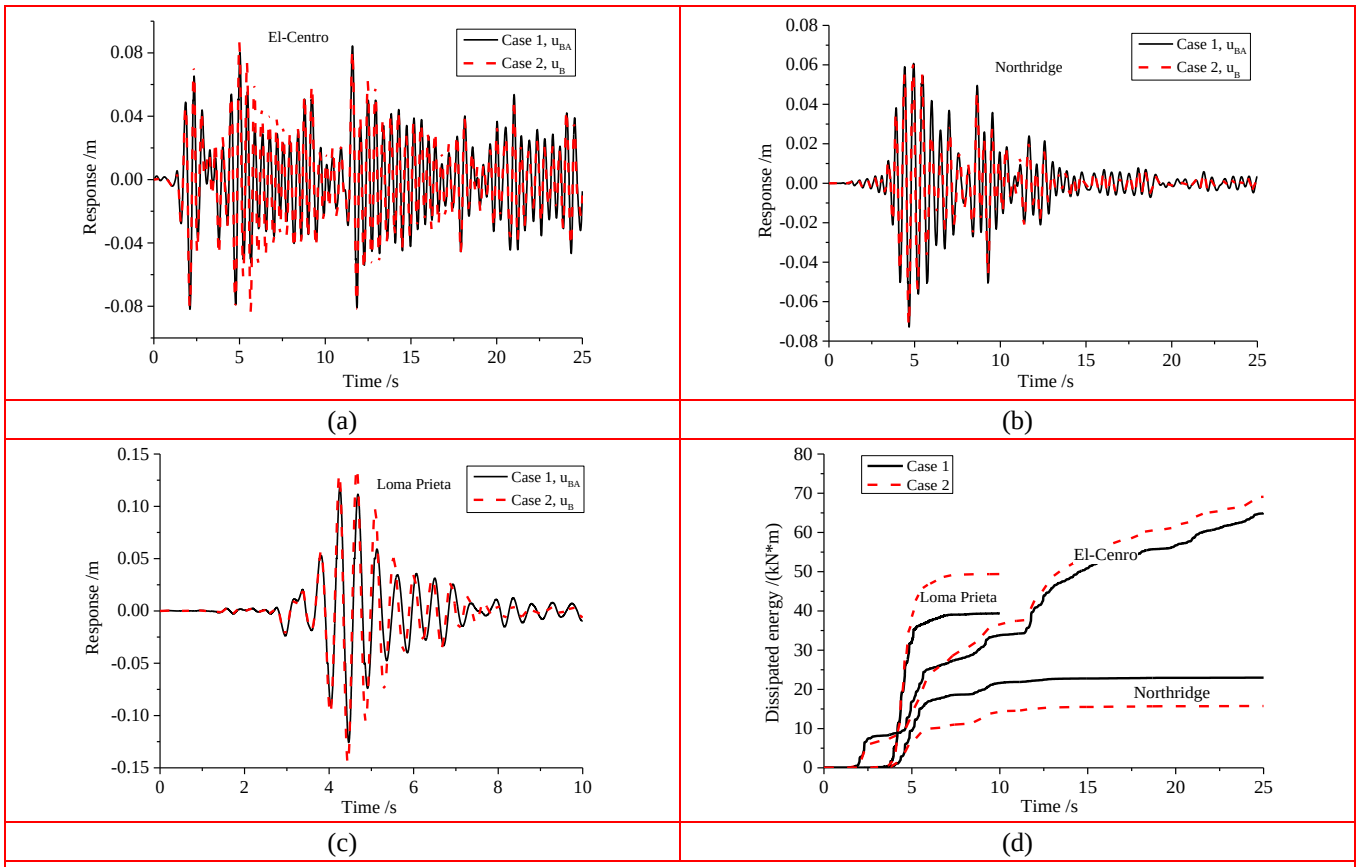

Fig. 4 Response and energy dissipation

The hysteresis curves of the friction component are shown in Fig. 3. It is observed that the stick-slip-hook component overcomes the stick, comes into the slip stage, and is finally hooked. Using the energy balance method and Eq. (5), the calculated EDRs for friction damping are approximately 1.4%, 2.7%, and 2.1% for the El-Centro, Northridge, and Loma Prieta earthquakes, respectively. Therefore, the total EDRs of the system are about 6.4%, 7.7%, and 7.1% for the El-Centro, Northridge, and Loma Prieta earthquakes, respectively; the latter values are the total damping ratios for Case 2. Then, the equivalent model in Case 2 is excited by the three earthquakes using these damping ratios, respectively. The responses and dissipated energy values of Cases 1 and 2 are shown in Fig. 4. It is found that there is a good agreement in terms of the response. This indicates that the EFDR that is approximately estimated by Eq. (5) is suitable for estimating the dynamic response using an additional damping. However, it should be noted that compared with Case 1, the accuracy for the energy dissipation estimation is not high (see Fig. 4(d)), especially for the Northridge and Loma Prieta earthquakes. The reason is that unlike the viscous damping, there will be no friction when the horizontal seismic force is small, and there is no energy dissipation; therefore, the friction damping exists only for a limited time during earthquakes. This leads to a reduction in the accuracy for the energy estimation. It also indicates that if the structure with the slip behavior at the bearings is equivalent to the base-fixed structure with additional damping, their estimated energy dissipation values may vary widely.

For the earthquake ground motion (El-Centro 1940 (E-W)), because the seismic force is overcome during the earthquake and the friction damping exists for most of the time, both the energy dissipation and the displacement can be better estimated.

4. Numerical model

4.1 Model description

A welded large-scale single-layer lattice dome was selected as the case study. The height is 22.5 m, the span length is 90 m, and the dome has a height-to-span ratio of $1/4$. The members used are steel pipes with a wall thickness of 0.01 m. The inner and outer radii of steel pipes are 0.145 m and 0.155 m, respectively. Fig. 5 shows the dome structure. The steel material has a yielding strength of 345 MPa and an elastic modulus of 2.1e11 $\mathrm{N/m^2}$. The stress-strain relationship of steel material is described by the elastic-perfectly plastic model. The finite element software *Perform-3D* was used to perform the static and transient analyses. Applied loads include: self-weight and seismic loads (three components). The self-weight of the dome is m_l =120 $\mathrm{kg/m^2}$, and it is assumed to be concentrated at the joints as masses. The total self-weight of the structure is 9.356e6 N. Each bearing has a pressure of 2.6e5 N under the gravity. Three earthquake records from the *Peer Strong Motion Database* were used, as listed in Table 3.

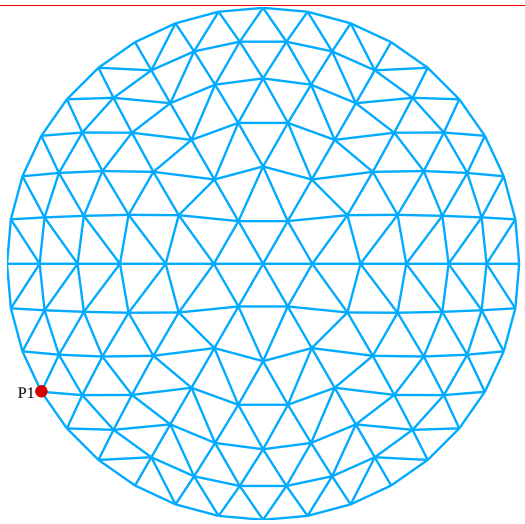

(a) Plane

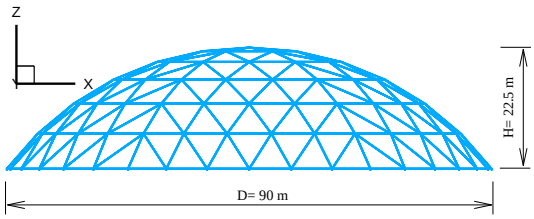

(b) Elevation

Fig. 5 Large-scale single-layer lattice dome

Table 3 Three selected ground motions

Ground motions	PGAs			Scale factor	Duration /s
	x	y	z		
GM(1)	-0.2808g	-0.2107g	-0.1781g	1	40
GM(2)	0.6177g	0.6711g	0.2842g	0.5	40
GM(3)	-0.2448g	-0.1515g	-0.1359g	1	40

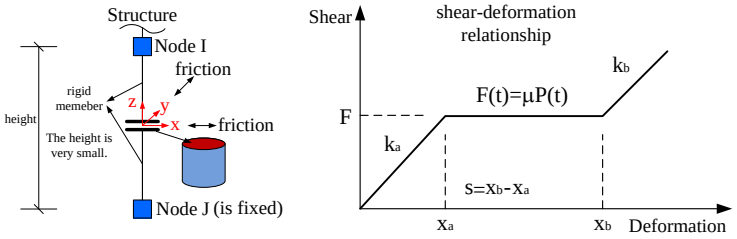

(a) modeling method for bearing (b) shear behavior of bearing

Fig. 6 Modeling method and shear-deformation relationship of the bearing

4.2 Modeling details

4.2.1 Stick-slip-hook component

In this study, the energy dissipation due to the friction at each bearing is equivalently modeled by a three-dimensional (3D) stick-slip-hook component with a pair of circular isotropic friction surfaces that can slide horizontally. The component has a very large stiffness in compression and a very small stiffness in tension. When the structure is uplifted, it means that there is zero friction in the component. A circular boundary is assumed for the component. The modeling method and shear behavior of the component are illustrated in Fig. 6. The symbols k_a, k_b, and s represent the initial stiffness (or stick stiffness), boundary stiffness, and slip distance of the bearing, respectively.

The component has the following characteristics (Zhang *et al.* 2019):

- In the initial stage, the load linearly increases with displacement due to the stick until the shear load reaches a value $F(t) = \mu P(t)$, where μ is the static friction coefficient and $P(t)$ is the time-varying normal force of the bearing. This is called the stick stage, where x_a is the length of the stick zone and x_b is the length of the stick-slip zone.
- After the shear load reaches a maximum value, the static friction force is overcome, and the bearing begins to slide. The energy dissipation then occurs, and this is called the slip stage.
- After the stick-slip distance x_b is reached, the bearing is restrained by the external support with a very large stiffness k_b to fix the bearing in order to avoid a large horizontal slippage.

The normal force $P(t)$ of the bearing is time-varying owing to the existence of the vertical component of seismic loads. The friction force $F(t)$ depends on the normal force and static friction coefficient; therefore, it is not a constant

during an earthquake. This is consistent with actual engineering scenarios. This friction characteristic of the bearing is considered in this study.

In practical engineering, the friction coefficient depends on the normal pressure, the slip rate, and the average surface temperature. To simplify the structural dynamic analysis, the friction coefficient had been assumed to be constant in previous studies. However, in this study, it is assumed that the friction coefficient decays exponentially from the static value to the slip value according to the following formula (Oden and Martins 1985).

$$\mu = \mu_k + (\mu_s - \mu_k)\exp(-d_c\dot{\gamma}_{eq}) \quad (6)$$

where μ_k is the slip friction coefficient; μ_s is the stick friction coefficient; d_c is an empirical decay constant; and $\dot{\gamma}_{eq}$ is the slip rate. This model can be used only with the isotropic friction. In general, the slip friction coefficient of the steel–steel contact surface ranges from 0.3 to 0.5, and the stick friction coefficient can be as high as 0.74 to 0.78 (Grigoriev and Meilikhov *et al*. 1997). Further, the static and kinetic friction coefficients of the non-steel–steel contact surfaces are larger than those of the steel–steel contact surfaces at the supports. Fig. 7 shows the slip rate-dependent friction coefficients with different decay constants, where the stick and slip friction coefficients are set as 0.75 and 0.45, respectively.

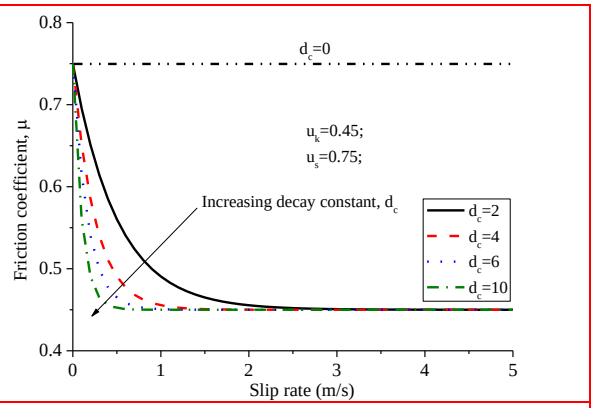

Fig. 7 Slip rate-dependent friction coefficient

4.2.2 Joint

For large-scale single-layer lattice domes, the members are welded to the hollow balls. Compared with the stiffness of the members, the stiffness of the welded balls is very large. These joints (or balls) are often referred to as stiff zones, as shown in Fig. 8(a). The stiffness of these joints significantly affects the performance of the structure. However, in previous studies involving finite element modeling, these balls were rarely considered.

For a specific welded ball, the range of the stiff zone L has been studied (Teng and Zhu *et al*. 2010) and is shown in Eq. (7).

$$L = R - 0.25d \quad (7)$$

where R is the outer radius of the welded hollow ball, and d is the outer diameter of the steel pipe. In this study, an equivalent method is used, as shown in Fig. 8(b). It is implemented by conducting two short members that have the section with the very large stiffness, and the length L at the ends of each steel pipe. In this study, the outer radius of the welded ball is designed as 0.45 m; therefore, according to Eq. (7), the length of the stiffness zone is approximately 0.37 m.

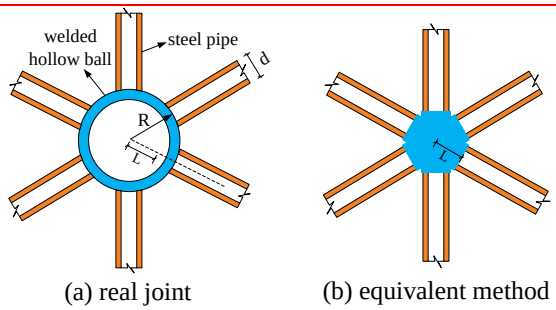

(a) real joint (b) equivalent method

Fig. 8 Schematic diagram of a joint

4.2.3 Member

The members in a dome are mainly subjected to the axial force, bending moment, and small shear force (Zhang and Han 2013). This is similar to the characteristics of column. Therefore, in this study, these members are modeled as column elements in finite element analysis. The section of steel pipe is modeled as a *Column Inelastic Fiber Section*, which can couple the behavior in the axial and bending directions. Therefore, the *Column Inelastic Fiber Section* can capture the nonlinear behavior of the fibers; however, it is assumed to be elastic for shear and torsion. In this study, the section of the member is specified as 12 fibers along the circumferential direction. The modeling method of the member is shown in Fig. 9. The whole component is composed of two stiff zones with a length of L, and a steel pipe with nonlinear characteristics. Each stiff zone has an annular cross-section with an outer radius r_a and a wall thickness of 0.06 m. The outer radius of the cross-section determines the stiffness of the stiff zone. The length of the steel pipe is L'.

In this study, $r_a = r$, $r_a = 2r$, and $r_a = 4r$ are discussed to analyze the effect of the structural stiffness on the respective EDRs.

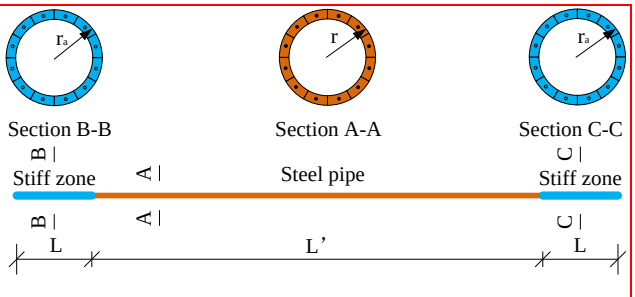

Fig. 9 Modeling method for the members

4.2.4 Damping model for structural dynamic analysis

The Rayleigh damping model is used to obtain the damping matrix, in which the i^{th} modal damping ratio ξ_i can be written as

$$\xi_i = \alpha \frac{T_i}{4\pi} + \beta \frac{\pi}{T_i} \quad (8)$$

where α, β, and T_i are the mass-proportional damping coefficient, stiffness-proportional damping coefficient, and the period of the ith mode, respectively. If the periods and damping ratios of two modes are defined, the damping coefficients can be determined.

The first damping ratio of the dome is usually related to the span length. Ikuo *et al.* (1997) gives the relationship between the first modal damping ratio and the span length, as shown in Eq. (9).

$$\xi_1 = 3/D \times 100\% \quad (9)$$

where ξ_1 and D are the first modal damping ratio and the span length of the dome, respectively.

of fixed supports can decrease the vibrating periods.

According to Table 4, $T_A \approx 0.75\ T_1$. To ensure that the modal damping ratio remains constant over a large frequency range (Huang and Richard *et al.* 2019), a damping ratio of 1% at $0.6T_1$ and T_1 is assumed in this study. According to Eq. (8), the calculated damping coefficients, α and β, are equal to 0.2873 and 3.26e-4, respectively. The damping ratio–period curve is shown in Fig. 10. It is observed that the minimum damping ratio is 0.97%, and the damping ratios for modes with periods in the range of $0.6T_1$ to T_1 are very close to 1% for the first 30 modes of the dome.

4.2.5 Estimation of friction damping ratio

The focus of this study is to estimate the friction damping at the bearings. When using Eq. (5) to quantify the EDR, the accuracy of the estimations also depends on the number of half waves N. In order to ensure accuracy, the quantification of equivalent viscous damping ratio, which is determined by Eq. (8), and which is approximately equal to 1% for each mode, is used as a reference to calculate the number of half waves.

Table 4 Periods of the dome (μ=0.45, k_a=1.17e8 N/m, and $r_a = 2r$)

Mode	1	2	3	4	5	6	7	8	9	10
Period /s	0.2734	0.2734	0.2342	0.2342	0.2341	0.2341	0.2327	0.2304	0.2304	0.2285
Mode	11	12	13	14	15	16	17	18	19	20
Period /s	0.2284	0.2274	0.2252	0.2252	0.2249	0.2232	0.2216	0.2216	0.2179	0.2179
Mode	21	22	23	24	25	26	27	28	29	30
Period /s	0.216	0.2151	0.2151	0.2096	0.2096	0.2094	0.2094	0.2086	0.2079	0.2064

Table 5 Periods of the dome (μ=0.45, k_a=1.17e8 N/m, and $r_a = r$)

Mode	1	2	3	4	5	6	7	8	9	10
Period /s	0.2836	0.2836	0.2446	0.2246	0.2437	0.2437	0.2437	0.2406	0.2406	0.239
Mode	11	12	13	14	15	16	17	18	19	20
Period /s	0.2378	0.2372	0.2354	0.2354	0.2353	0.2329	0.2312	0.2312	0.2279	0.2279
Mode	21	22	23	24	25	26	27	28	29	30
Period /s	0.2264	0.2249	0.2249	0.2194	0.2194	0.2191	0.2191	0.2179	0.2174	0.2169

Table 6 Periods of the dome (with fixed supports and $r_a = 2r$)

Mode	1	2	3	4	5	6	7	8	9	10
Period /s	0.259	0.259	0.2304	0.2304	0.2293	0.2276	0.2276	0.2258	0.2258	0.2253
Mode	11	12	13	14	15	16	17	18	19	20
Period /s	0.2227	0.2215	0.2203	0.2203	0.2194	0.2189	0.2153	0.2153	0.2131	0.2131
Mode	21	22	23	24	25	26	27	28	29	30
Period /s	0.212	0.207	0.207	0.2065	0.2065	0.202	0.202	0.2013	0.2005	0.1999

For the welded steel structures, there is no friction in joints. Because the damping at the bearings is directly modeled using the stick-slip-hook components, the welded large-scale single-layer dome has a structural damping ratio that is much lower than that given by Eq. (9). Based on the rules of thumb (Deierlein and Reinhorn *et al.* 2010), in this study, the damping ratio is set to 1% at T_A and T_B, and includes the material damping.

In this study, the first 50 modes of the dome are used in the dynamic analyses. Here, only the first 30 modal periods of the dome with the bearings having a constant friction coefficient are listed in Table 4. For comparison purposes, the first 30 modal periods of the dome with a smaller joint stiffness ($r_a = r$) and fixed supports are also given, respectively, as listed in Tables 5 and 6. According to the tables, it is observed that the decrease in the joint stiffness increases the vibrating periods of the structure, and the use

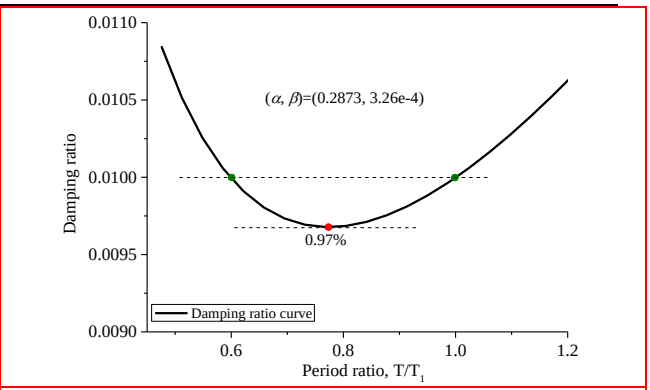

Fig. 10 Damping ratio–period curve

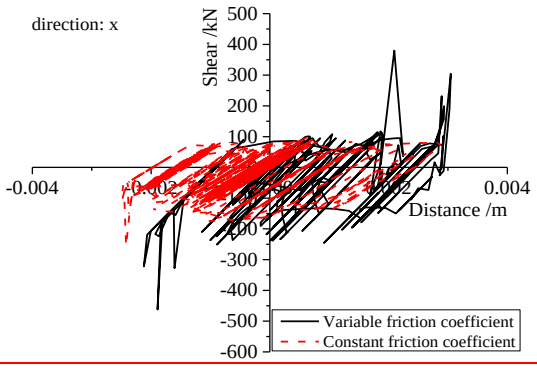

(a)

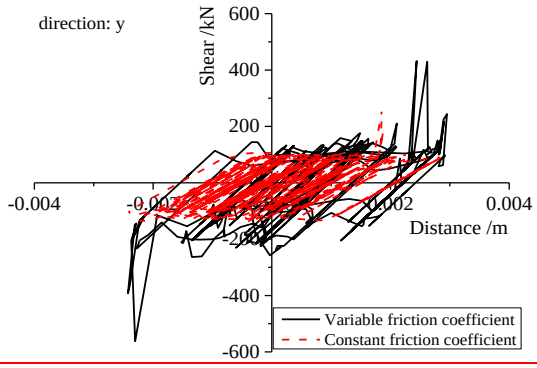

(b)

Fig. 11 Hysteretic loops of the bearing at Position P1 under GM(1)

Table 7 Energy dissipation and EDR of the bearing at position P1

Cases	Variable friction coefficient		Constant friction coefficient	
	Energy dissipation	Equivalent damping ratio	Energy dissipation	Equivalent damping ratio
Value	4437.7 N*m	2.3e-4	4794.5 N*m	4.5e-4

The specific estimation process is as follows:

- The number of half waves N is adjusted so that the modal damping ratio calculated using Eq. (5) is close to 1%.
- After that, the EFDR is obtained using the above number of half waves and Eq. (5).

Another simple method can calculate the EFDR, and it is given as follows:

$$\xi_f = \xi_v \frac{E_{d,f}}{E_{d,v}} \tag{10}$$

where ξ_f, ξ_v, $E_{d,v}$, and $E_{d,f}$ are the equivalent friction damping ratio, equivalent viscous damping ratio, energy dissipation due to viscous damping, and energy dissipation due to friction damping, respectively.

5. Results

Based on an explicit modeling method for bearings with a small slip distance, the welded large-scale single-layer lattice dome subjected to earthquake ground motions is analyzed using the energy balance concept. Both the variable coefficient and the constant friction coefficient are considered. In this study, we consider the effect of the normal force on the friction force of the bearing.

For each bearing with a variable friction coefficient, the following parameters are assumed:

$$\begin{cases} \mu = 0.45 + (0.75 - 0.45)exp\,(-10\dot{\gamma}_{eq}) \\ x_a = 0.001 \text{ m} \\ s = 0.002 \text{ m} \\ k_a = 1.95\text{e}8 \text{ N/m} \\ k_b = 5\text{e}9 \text{ N/m} \end{cases}$$

where the stick stiffness k_a is defined by the stick distance x_a and static friction force under the gravity load.

For each bearing with a constant friction coefficient, the following parameters are assumed:

$$\begin{cases} \mu = 0.45 \\ x_a = 0.001 \text{ m} \\ s = 0.002 \text{ m} \\ k_a = 1.17\text{e}8 \text{ N/m} \\ k_b = 5\text{e}9 \text{ N/m} \end{cases}$$

5.1 Horizontal hysteretic behaviors of bearing

Fig. 11 shows the horizontal hysteretic behaviors of the bearing at Position P1 (see Fig. 5) under GM(1). It is found that the horizontal seismic force in both directions makes the bearing overcome the stick-slip and enter the hooked stage, which leads to a sharp increase in the lateral force of the bearing. Owing to the existence of a variable vertical seismic force, which leads to an alternating normal and friction forces on the bearing, the relationship between the friction force of the bearing and the sliding distance is different from that shown in Fig. 3. These hysteretic loops result in the energy dissipation.

According to the following equation, the EDR ξ_b of the single bearing contributing to the total structural EDR can be quantified by the following equation.

$$\xi_b = \frac{1}{4\pi N} E_{d,b} / \bar{E}_s \tag{11}$$

where $E_{d,b}$ is the energy dissipation of the bearing resulting from friction. Table 7 lists the energy dissipation and EDRs of the bearing. It is observed that the energy dissipation of the bearing with a variable friction coefficient is slightly less than that of the bearing with a constant friction coefficient. However, the EDRs in both cases are different, and are approximately 2.3e-4 and 4.5e-4, respectively; the reason is that the value of EDR also depends on the strain energy parameter of the structure.

5.2 Energy dissipation demand and energy dissipation ratio

The structural damping ratio that can be used in elastoplastic dynamic analysis should be determined based

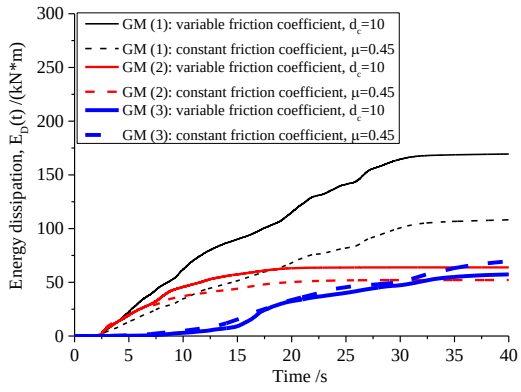

(a)

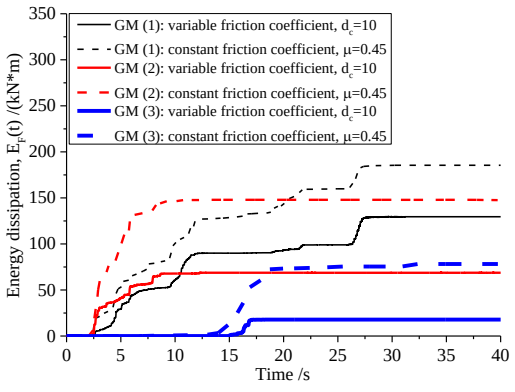

(b)

Fig. 12 Energy dissipation demands of the dome owing to: (a) modal damping and (b) friction at the bearings

on the energy dissipation caused by the viscous damping and friction if the energy dissipation is not directly modeled. In existing literature, there has been more focus on E_D in Eq. (3). However, to estimate the total EDR, E_F needs to be found owing to its direct relationship with the structural friction damping ratio.

Fig. 12 illustrates the energy dissipation of bearings with $d_c = 10$ and $\mu = 0.45$ under three earthquake ground motions. The modal damping has been dissipating the input energy of the structure during an earthquake, and the energy curve increases slowly, as shown in Fig. 12(a). However, the friction at the bearings dissipates the input energy only for a limited period of time; therefore, the energy dissipation increases in a step-by-step manner because the friction mechanism at the bearings needs to be activated by the lateral seismic force, as shown in Fig. 12(b). As expected, the friction energy dissipation of the structure with a variable friction coefficient is significantly less than that of the structure with a constant friction coefficient.

Fig. 13 shows the energy dissipation ratios E_F/E_I for $d_c = 10$ and $\mu = 0.45$. It is observed that the bearings with a constant friction coefficient lead to a larger energy dissipation ratio compared with those that have a variable friction coefficient. Generally, these ratios are within the range of 24% to 74%. The results indicate that the friction mechanism at the bearings should be considered in dynamic analysis because it is an important damping source.

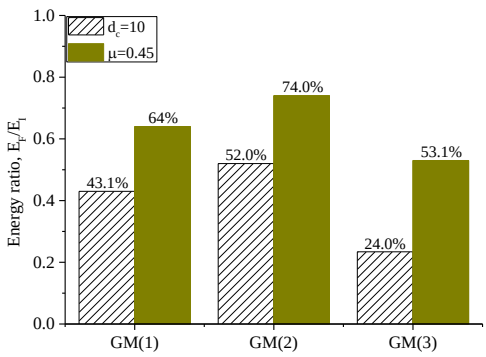

Fig. 13 Energy dissipation ratio E_F/E_I

5.3 EDR resulting from friction at bearings

Based on the approximate method employed in this paper, the EDRs resulting from the friction at the bearings are quantified by considering a variable friction coefficient and constant friction coefficient, respectively, as shown in Fig. 14. It should be noted that these EDRs exclude the damping ratios caused by the hysteretic energy dissipation, and they are the average damping ratios during earthquakes. It is observed that the selection for the friction coefficient has an obvious effect on the EDR. Clearly, the constant friction coefficient leads to a larger EDR than the variable friction coefficient. If these EDRs are applied to the structural dynamic analysis, attention should be given to the selection of the friction coefficient.

At present, there are limited estimation methods that can determine the friction damping ratio with high accuracy, especially for structures that are subjected to earthquake ground motions. Generally, the method described by Eqs. (4) and (5) based on the energy balance concept is widely accepted for estimating EDRs. However, caution must be exercised in the use of these friction damping ratios when predicting the dynamic response in engineering practice because of the amplitude-dependent characteristic of the friction damping. This is discussed in the following section.

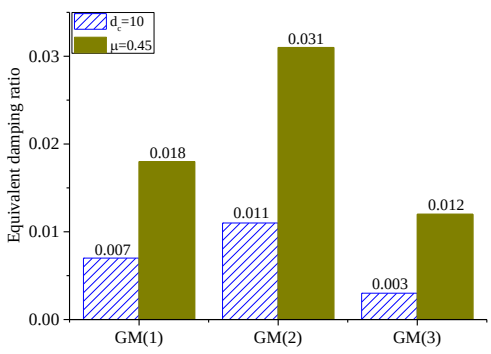

Fig. 14 EDR at the bearings of the dome

6. Parametric study

This section investigates the effects of different parameters on energy dissipation and the EDR at the bearings of the dome. The focus is on the amplitude-

dependent characteristic of EDRs.

6.1 Effect of the friction coefficient on nonlinear energy dissipation at bearings

The energy dissipation curves of the dome due to friction under GM(1) and GM(2) are plotted in Fig. 15. When the smaller friction coefficient is used, it is observed that a larger amount of energy is dissipated, and the energy dissipated by the bearings with $\mu = 0.75$ accounts for only 58% and 28% of the energy dissipated by the bearings with $\mu = 0.45$ under GM(1) and GM(2), respectively. This shows that the friction damping mechanism in the bearing with a larger friction coefficient is not easily activated, resulting in less energy dissipation, which is consistent with the actual situation. For example, when the support is completely fixed, it means that the bearing has an infinite friction coefficient; however, it does not dissipate the input energy through friction.

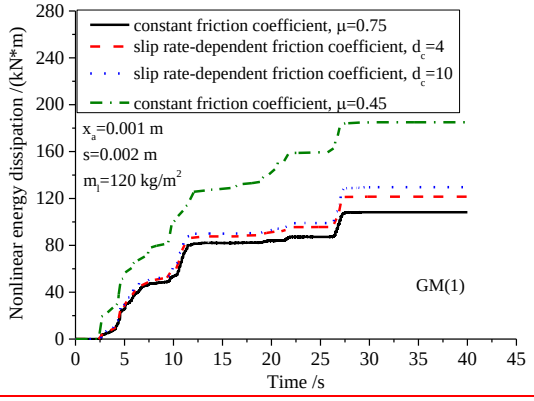

(a)

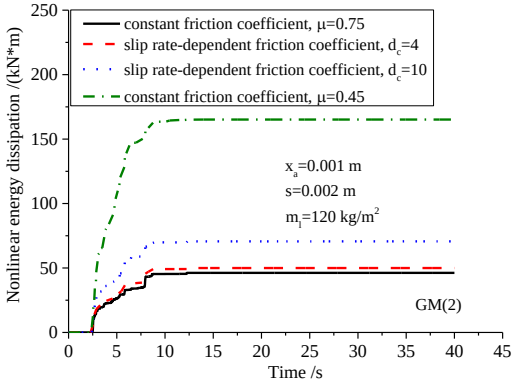

(b)

Fig. 15 Energy dissipation of bearings with different friction coefficients

Fig. 16 shows the energy dissipation ratios E_F/E_I with different friction coefficients. Although the bearings have a very small slip distance, it is found that the energy dissipated by friction accounts for a large proportion of the total input energy. Moreover, it is observed that the energy dissipation ratio increases with a decrease in the friction coefficient.

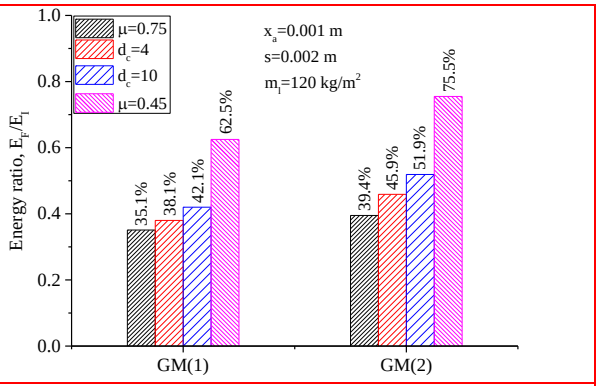

Fig. 16 Energy dissipation ratio E_F/E_I with different friction coefficients

6.2 Effect of friction coefficient on EDR

As shown in Figs. 15 and 16, different friction coefficients have an obvious effect on nonlinear energy dissipation, as well as on the EDR of the structural systems. This section investigates the EDR of bearings with different friction coefficients under GM(1). The bearings have the characteristics shown in Fig. 17. Here, it is assumed that the stick distance is 0.001 m for the three cases.

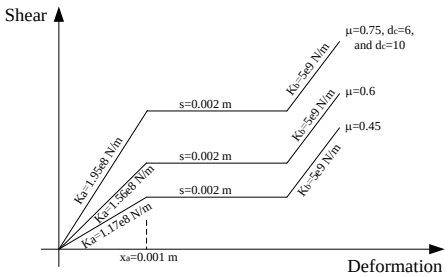

Fig. 17 Characteristics of the bearings for different stick stiffness values

Fig. 18 shows the variation trend of the EDRs caused by friction with the scale factors of the ground motion. It is found that the EDRs are amplitude-dependent, and they do not exist when the scale factor is very small. For the large scale factors, the EDRs first increase with the increase in the scale factor, and then they begin to decrease slowly. An important observation is that the maximum EDRs occur in the elastic range of the structure.

For the cases with constant friction coefficients, it is observed that the damping ratios increase significantly with a decrease in the friction coefficient in phase 1; however, the damping ratios increase slightly with a increase in the friction coefficient in phase 2.

For the cases with variable friction coefficients, the variation trend of the EDRs is the same as that of the EDRs that are estimated using constant friction coefficients. The EDRs that are estimated using larger friction coefficients (such as $\mu = 0.75$ ($d_c = 0$), $d_c = 6$, and $d_c = 10$) vary only slightly. Overall, the maximum EDRs range from around 3% to 4.3%.

6.3 Effect of slip distance on EDR

The effect of different slip distances on the EDR is discussed in this section. The slip distances $s = 0.002$ m, 0.004 m, and 0.006 m are assumed. The stick distance x_a is set to 0.001 m. The static load of the structure and the

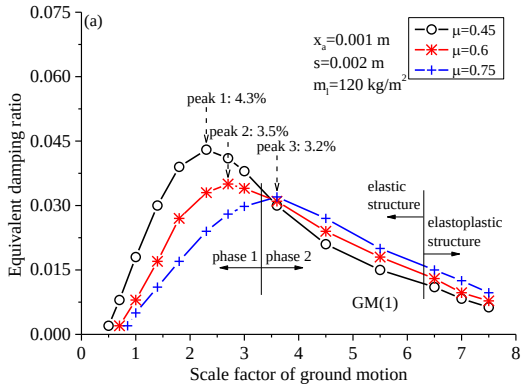

(a)

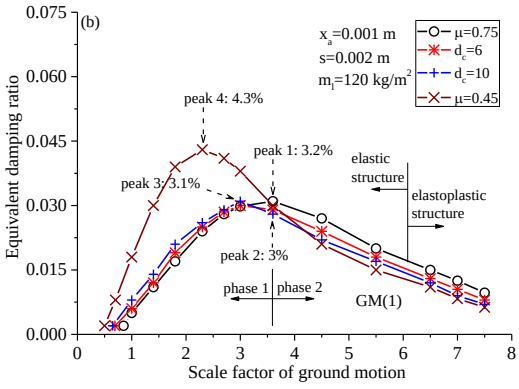

(b)

Fig. 18 EDRs of bearings with different friction coefficients

static friction coefficient of bearings are used to calculate the stick stiffness. Therefore, the bearings have the characteristics shown in Fig. 19. EDRs with both constant friction coefficient and variable friction coefficient were investigated, as shown in Fig. 20. It is observed that there is no clear difference in the EDRs for small scale factors (phase 1); however, the EDRs have a significant difference with the increase of the scale factors (phase 2) and they increase with the increase in the slip distance. The maximum EDRs occur in the elastic stages of the structures for all cases. It is also found that the sliding friction with a larger slip distance can better dissipate the input seismic energy, so the structure has a better seismic performance.

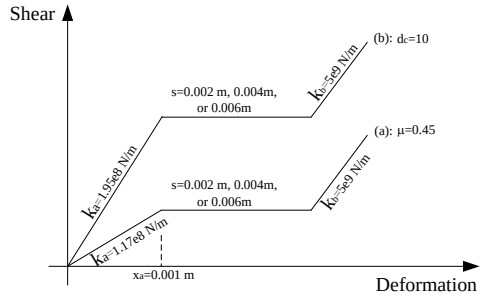

Fig. 19 Characteristics of bearings with different slip distances

6.4 Effect of roof load on EDR

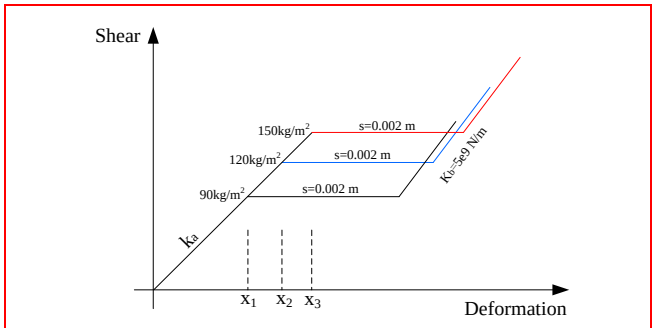

Fig. 21 Characteristics of bearings for different stick distance values

Different roof loads can result in different bearing pressures, and accordingly, the sliding friction force (or shear) of the bearing varies according to Fig. 6, which leads to varying stick distance value x_a. In this study, the roof loads $m_l = 90$, 120, and 150 kg/m^2 were selected to investigate the effects of the roof load on the EDR. Here, the stick stiffness was set to k_a=1.17e8 N/m for the cases with a constant friction coefficient $\mu = 0.45$, and k_a=1.95e8 N/m for the cases with a variable friction coefficient $d_c = 10$. The characteristics of the bearings are shown in Fig. 21. The stick distances x_1, x_2, and x_3 are respectively 7.5e-4 m, 0.001 m, and 1.25e-3 m under the

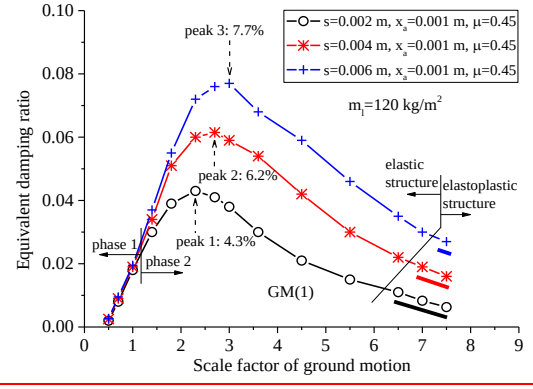

(a)

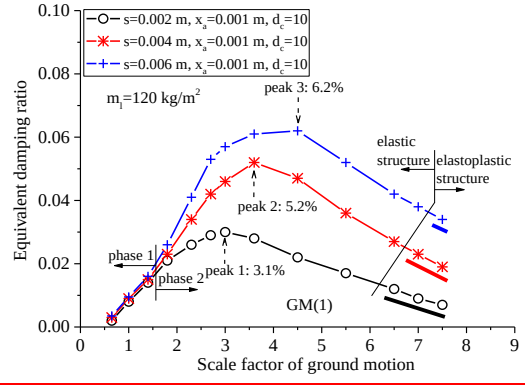

(b)

Fig. 20 Equivalent damping ratios of bearings with different slip distances

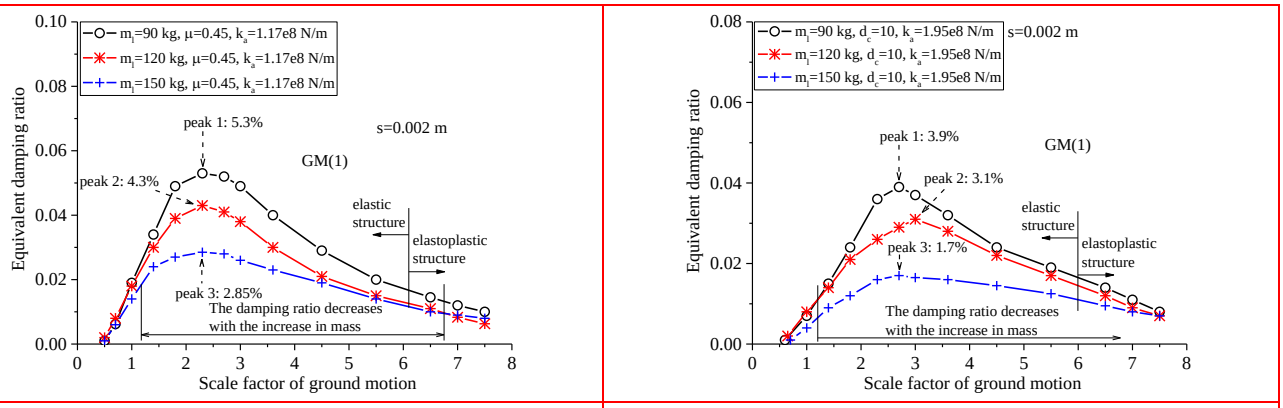

(a) (b)

Fig. 22 Equivalent damping ratios of bearings of the dome with different roof loads

above static loads.

The EDRs with different roof loads are shown in Fig. 22. It is observed that the EDRs decrease with an increase in the roof load (or stick distance) for both cases. However, there is no obvious difference in these damping ratios for small scale factors. The peaks of the EDRs with constant friction coefficients are significantly larger than those with variable friction coefficient. Generally, these damping ratios vary from around 1.7% to 5.3% for all cases. In addition, it is also observed that they tend to converge with the increase of the scale factors.

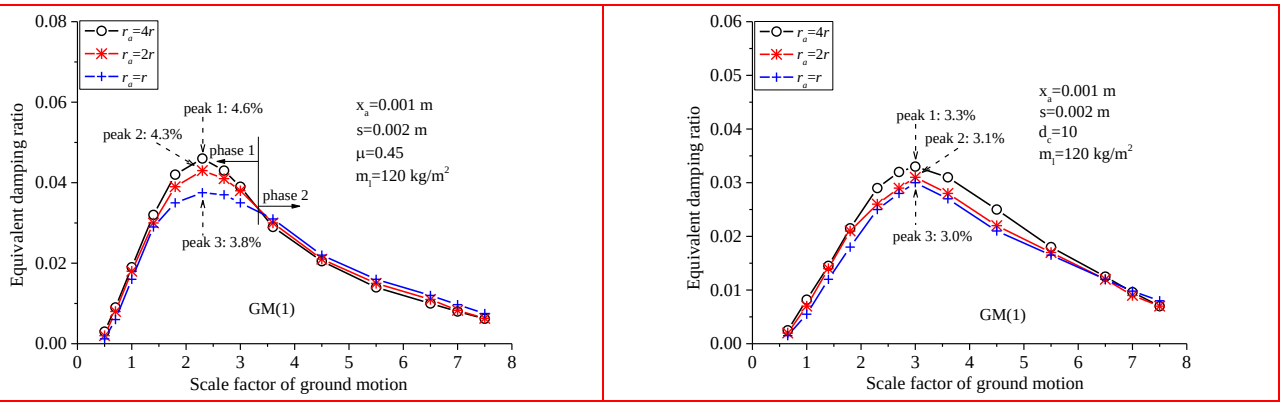

(a) (b)

Fig. 23 Equivalent damping ratios of bearings of the dome with different joint stiffness values

6.5 Effect of structural stiffness on EDR

According to Eqs. (4) and (5), the EDR of a structure is related to the structural strain energy, while the structural strain energy is affected by the structural stiffness. As discussed in *Sections 4.2.2* and *4.2.4*, the stiffness of the joints significantly impacts the stiffness of the whole structure. This study considers three joint stiffness values. The EDRs with different joint stiffness values are shown in Fig. 23. It is observed that the EDRs in phase 1 for a constant friction coefficient increase with the increase in the joint stiffness; however, it appears that the joint stiffness only has an obvious effect on the EDRs around the EDR peak, but there is no obvious effect on the other EDRs. For the cases with a variable friction coefficient, the variation of the EDRs is the same as that of the EDRs that are estimated using a constant friction coefficient.

7. Discussion: Friction damping mechanism and EDRs

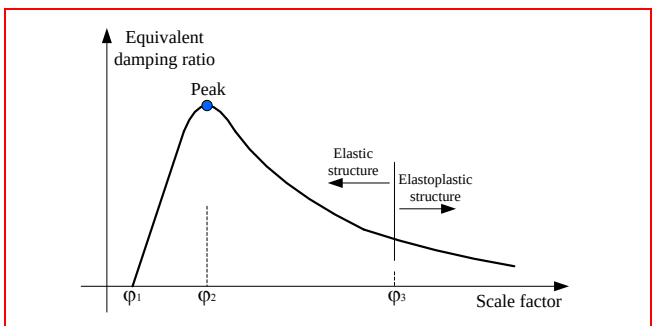

Fig. 24 Equivalent damping ratio model

Based on the above analysis, the EDR caused by friction at bearings is amplitude-dependent, and it changes with the intensity of the ground motions. The relationship between the EDR and the scale factor of the ground motion can be described in Fig. 24, where φ_1 is the minimum scale factor

of the ground motion required for the activation of the friction mechanism; φ_2 is the scale factor of the ground motion when the peak EDR is reached; and φ_3 is the scale factor of the ground motions when the structure enters the elastoplastic stage.

In the structures subjected to earthquake ground motions, before the sliding between interfaces can be activated, the necessary shear energy must first be reached to overcome the stick force. After the scale factor reaches φ_1, the EDR increases rapidly with the increase in the scale factor until it reaches the maximum, and then the EDR decreases slowly. The model for the EDR shows complex characteristics. It is not a constant during an earthquake. Based on Eq. (5), the complex characteristics of the EDR model are further investigated from an energy perspective. Fig. 25 shows the energy dissipation values and strain energy parameters used to estimate the EDRs under different scale factors. A constant friction coefficient $\mu = 0.45$ is used. For small scale factors, it is observed that both the energy dissipation and strain energy parameter increase slowly; when the scale factor reaches a value, the ratio of the nonlinear dissipated energy and the elastic stored energy reaches the maximum; after that, the strain energy parameter of the structure increases rapidly as the scale factor increases, while the energy dissipation still increases slowly. This leads to the EDR characteristics shown in Fig. 24.

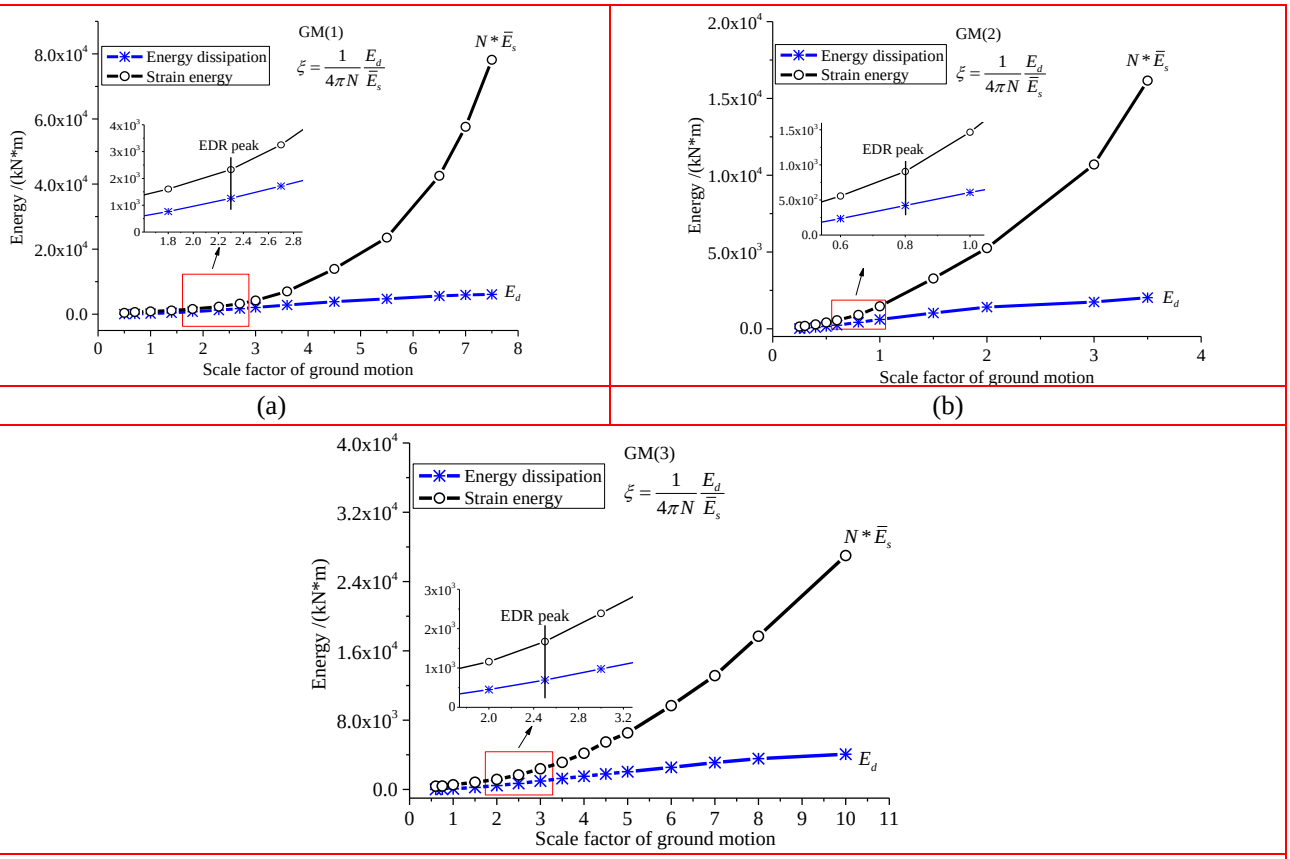

Fig. 25 Energy dissipation and strain energy parameter

8. Conclusions

At present, the friction damping at the bearings of the domes subjected to earthquake ground motions has not been extensively studied and quantified. In this paper, the energy loss due to friction at the bearings of a welded large-scale single-layer lattice dome was equivalently modeled by the three dimensional stick-slip-hook components. The EDRs of the dome subjected to earthquake ground motions were quantified using an approximate method based on the energy balance concept. The different friction coefficients of the contact surfaces and the different joint stiffness values of the members were considered. As a result, the complex friction behavior and energy loss between contact surfaces can be investigated in detail. A parametric analysis showed the complex relationship between the EDR and the intensity of the ground motion. It was observed that the EDR is amplitude-dependent, and it first increases with the increase in the intensity of the ground motion, and after the critical ground motion intensity is reached, it begins to decrease slowly. This observation provides researchers and engineers with a better understanding of the essential characteristics of the EDRs due to friction under earthquake ground motions. Finally, based on a discussion, the friction damping mechanism at the bearings was described in detail.

Acknowledgments

The authors gratefully acknowledge the financial support provided by the National Key Research and

Development Program of China (Grant No. 2018YFC1504304), the Key Project of the Natural Science Foundation of Tianjin (Grant No. 19JCZDJC39300), and the National Natural Science Foundation of China (Grant No. 51878433).

References

Beards, C.F. (1996), *Structural Vibration: Analysis and Damping*, Butterworth-Heinemann Elsevier Ltd, Oxford, United Kingdom.

Chopra, A.K. (2011), *Dynamics of Structures* (4th Ed), Prentice Hall, USA.

Clarence, W.S. (2005), *Vibration and Shock Handbook*, CRC Press, Boca Raton, Florida, USA.

Computers and Structures, Inc. (CSI). (1995), CSI Perform-3D User Guide, Berkeley, California, USA.

Deierlein, G.G., Reinhorn, A.M. and Willford, M.R. (2010), "Nonlinear structural analysis for seismic design: a guide for practicing engineers", NEHRP Seismic Design Technical Brief No. 4; National Institute of Standards and Technology, Department of Commerce, USA.

Dwairi, H.M., Kowalsky, M.J. and Nau, J.M. (2007), "Equivalent damping in support of direct displacement-based design", *Journal of Earthquake Engineering*, **11**(4), 512–530. https://doi.org/10.1080/13632460601033884

Feeny, B.F. and Liang, J.W. (1996), "A decrement method for the simultaneous estimation of coulomb and viscous friction", *Journal of Sound and Vibration*, **195**(1), 149–154. https://doi.org/10.1006/jsvi.1996.0411

Goodman, L.E. (2002), *Material Damping and Slip Damping (in shock and vibration handbook)* (5th Ed.), McGraw-Hill, New York, USA.

Gounaris, G.D. and Anifantis, N.K. (1999), "Structural damping determination by finite element approach", *Comput. Struct.*, **73**(1–5), 445–452. https://doi.org/10.1016/s0045-7949(98)00257-0

Gounaris, G.D., Antonakakis, E. and Papadopoulos, C.A. (2007), "Hysteretic damping of structures vibrating at resonance: An iterative complex eigensolution method based on damping-stress relation", *Comput. Struct.*, **85**(23–24), 1858–1868. https://doi.org/10.1016/j.compstruc.2007.02.026

Grigoriev, I.S., Meilikhov, E.Z. and Radzig, A.A. (1997), *Handbook of Physical Quantities*, CRC Press, Boca Raton, Florida, USA.

Huang, Y.L., Richard, S. and Michael, W. (2019), "A damping model for nonlinear dynamic analysis providing uniform damping over a frequency range", *Computers and Structures*, **212**, 101–109. https://doi.org/10.1016/j.compstruc.2018.10.016

Ikuo, T., Tatsuo, H., Yoshimichi, A. and Satoshi, F. (1997), "Vibration tests on a full-size suspen-dome structure", *Int. J. Space Struct.*, **12**(3-4), 217–224. https://doi.org/10.1177/026635119701200310

Jacobsen, L.S. (1930), "Steady forced vibrations as influenced by damping", *Trans ASME*, **52**(1), 169–181.

Jennings, P.C. (1968), "Equivalent viscous damping for yielding structures", *Journal of Engineering Mechanics Division (ASCE)*, **94**(1), 103–116.

Kareem, A. and Gurley, K. (1996), "Damping in structures: its evaluation and treatment of uncertainty", *Journal of Wind Engineering & Industrial Aerodynamics*, **59**(2-3), 131–157. https://doi.org/10.1016/0167-6105(96)00004-9

Kwan, W.P. and Billington, S.L. (2003), "Influence of hysteretic behavior on equivalent period and damping of structural systems", *Journal of Structural Engineering (ASCE)*, **129**(5), 576–585. https://doi.org/10.1061/(asce)0733-9445(2003)129:5(576)

Lazan, B.J. (1968), *Damping of Materials and Members in Structural Mechanics*, Pergamon Press, London, United Kingdom.

Liu, T., Zordan, T., Zhang Q. and Briseghella B. (2015), "Equivalent viscous damping of bilinear hysteretic oscillators", *J Struct Eng*, **141**(11), 06015002. https://doi.org/10.1061/(asce)st.1943-541x.0001262

Oden, J.T. and Martins, J.A.C. (1985), "Models and computational methods for dynamic friction phenomena", *Computer Methods in Applied Mechanics and Engineering*, **52**(1-3), 527–534. https://doi.org/10.1016/0045-7825(85)90009-x

Papagiannopoulos, G.A. (2018), "Jacobsen's equivalent damping concept revisited", *Soil Dynamics and Earthquake Engineering*, **115**, 82–89. https://doi.org/10.1016/j.soildyn.2018.08.001

Papagiannopoulos, G.A. and Beskos, D.E. (2010), "Towards a seismic design method for plane steel frames using equivalent modal damping ratios", *Soil Dyn Earthq Eng*, **30**(10), 1106–1118. https://doi.org/10.1016/j.soildyn.2010.04.021

Petrini, L. and Maggi, C. *et.al.* (2008), "Experimental verification of viscous damping modeling for inelastic time history analyzes", *Journal of Earthquake Engineering*, **12**(S1), 125–145. https://doi.org/10.1080/13632460801925822

Sheen, R.L. (1984), "Experimental measurement of material damping for space structures in simulated zero-G", Rept No. AFIT/CI/ NR-83-84T; Wright-Patterson AFB: Air Force Inst. of Tech., OH, U.S.

Tamura, Y. (2012), "Amplitude dependency of damping in buildings and critical tip drift ratio", *International Journal of High-Rise Buildings*, **1**(1), 1–13. https://doi.org/10.1061/41000(315)39

Teng, J., Zhu, Y.H. and Zhou, F. (2010), "Finite element model updating for large span spatial steel structure considering uncertainties", *J. Cent. South Univ. Technol.*, **17**(4), 857–862. https://doi.org/10.1007/s11771-010-0567-4

Zhang, H.D. and Han, Q.H. (2013), "A numerical investigation of seismic performance of large span single-layer latticed domes with semi-rigid joints", *Structural Engineering and Mechanics*, **48**(1), 57–75. https://doi.org/10.12989/sem.2013.48.1.057

Zhang, H.D. and Wang, Y.F. (2012a), "Energy-based numerical evaluation for seismic performance of a high-rise steel building", *Steel and Composite Structures*, **13**(6), 501–519. https://doi.org/ 10.12989/scs.2012.13.6.501

Zhang, H.D. and Wang, Y.F. (2012b), "Energy-based study on the dynamic elastic plasticity seismic capacity of a high-rise steel structure", China Civil Engineering Journal, **45**(6), 65–73. (in Chinese) https://doi.org/10.15951/j.tmgcxb.2012.06.015

Zhang, H.D., Han, Q.H., Wang, Y.F. and Lu, Y. (2016), "Explicit modeling of damping of a single-layer latticed dome with an isolation system subjected to earthquake ground motions", *Eng. Struct.*, **106**, 154–165. https://doi.org/10.1016/j.engstruct.2015.10.027

Zhang, H.D., Wang, Y.F. and Han, Q.H. (2015), "Nonlinear material loss factors of single-layer latticed domes subjected to earthquake ground motions", *Journal of Structural Engineering (ASCE)*, **141**(7), 04014181. https://doi.org/10.1061/(asce)st.1943-541x.0001149

Zhang, H.D., Zhu, X.Q., Li, Z.X. and Yao, S. (2019), "Displacement-dependent nonlinear damping model in steel buildings with bolted joints", *Advances in Structural Engineering*, **22**(5), 1049–1061. https://doi.org/10.1177/1369433218804321